Int. J. Solids Structures Vol. 28, No. 6, pp. 751–768, 1991
Printed in Great Britain.

0020–7683/91 $3.00 + .00

ELASTODYNAMIC RESPONSES DUE TO ANTI-PLANE POINT IMPACT LOADINGS ON THE FACES OF AN INTERFACE CRACK ALONG DISSIMILAR ANISOTROPIC MATERIALS

M. K. KUO and S. H. CHENG
Institute of Applied Mechanics, National Taiwan University, Taipei, Taiwan 106, R.O.C.

(*Received* 2 *April* 1990; *in revised form* 19 *January* 1991)

Abstract—The transient elastodynamic fields and the stress intensity factor of a semi-infinite interface crack lying between dissimilar anisotropic half planes are analyzed. The crack is subjected to a pair of suddenly-applied anti-plane concentrated point loadings on its faces, at a distance l away from the crack tip. The problem is first transformed into one with the interface crack lying between dissimilar isotropic half planes by a transformation of relevant coordinates and parameters. The crucial steps in the analysis are then the direct application of integral transforms together with the Wiener–Hopf technique and the Cagniard–de Hoop method, which were previously believed not to be appropriate. Exact expressions are obtained for the resulting mode-III stress intensity factors, $\hat{K}_{III}$, and radiated stress fields as functions of time. The numerical results are presented for both anti-symmetric and symmetric loadings. The results show that $\hat{K}_{III}$ is almost constant with time, but experiences discontinuity at a time $t = s_2 l$, which is the arrival time of the cylindrical wave emitted from the point loading of the slower medium on the crack tip. Moreover, $\hat{K}_{III}$ jumps to the appropriate static value (at $t = s_2 l$) for the case of anti-symmetric loading but not for the case of symmetric loading. The results also show that the transient radiated stress component $\hat{\sigma}_{\theta t}$ has fewer discontinuities and fewer singularities than other stress components. On the other hand, the order of magnitude of $\hat{\sigma}_{\theta t}$ is one less than that of $\hat{\sigma}_{rt}$.

1. INTRODUCTION

In recent years, the increasing uses of composites have generated considerable research efforts in the modeling, testing and analysis of laminated media. These materials differ from traditional isotropic homogeneous materials in their anisotropy and multi-layeredness. Contiguous layers of composite laminates, however, may not be properly adhered, and the interfaces may contain flaws which can lead to serious degradation in load-carrying capacity.

In this paper we are interested in the anti-plane transient elastodynamic responses and stress intensity factors of a semi-infinite crack lying along the interface of an anisotropic bimaterial. The crack faces are suddenly loaded by a pair of concentrated anti-plane point forces which are located at a distance of l away from the crack tip. The materials are assumed to possess certain material symmetry and the crack plane coincides with one of the planes of material symmetry, so that the in-plane and the anti-plane motions are not coupled. Stresses in such materials due to anti-plane shear deformations are described by three elastic constants (three shear moduli rather than one as for isotropic solids). Hence, the wavefronts of anti-plane shear waves are ellipses rather than circles. The question of elliptical anisotropy has been discussed in some detail by Helbig (1983). For a recent review on wave motions in anisotropic media, refer to Crampin's work (1981).

It is well known that in general the near-tip stresses of an in-plane interface crack possess oscillatory singularities if the crack faces are assumed traction free (England, 1965). Such oscillatory singularities lead to the contradiction that the crack faces interpenetrate each other. In contrast to the in-plane cases, the near-tip stresses of anti-plane shear interface cracks exhibit an inverse square-root singularity as for cracks in homogeneous solids and the contradiction of the crack faces' interpenetration does not appear (Sih and Chen, 1981). Consequently, the stress intensity factor of the anti-plane interface crack is well defined.

The analyses of the paper are based first on the observation that anti-plane shear deformations in an anisotropic solid can be deduced from the corresponding deformations of an isotropic solid by a transformation of relevant coordinates and parameters. The

corresponding relations have also been noted by several researchers, e.g. Markenscoff and Ni (1984), Achenbach and Kuo (1986), Ma (1989) and Wu and Chiu (1989). In particular, Markenscoff and Ni (1984) and Achenbach and Kuo (1986) analyzed the elastodynamic responses of a homogeneous anisotropic solid and a cracked homogeneous transversely-isotropic half plane, respectively. Ma (1989) and Wu and Chiu (1989), on the other hand, were concerned with static anisotropic composite wedges and the static interface crack, respectively. Based on this observation, analyses of the interface crack between dissimilar anisotropic solids are converted into that between dissimilar isotropic solids.

In some respects, the present problem can be regarded as a mode-III interface crack analogue of those considered by Freund (1974) (hereafter referred to as problem A) and Brock (1982), where mixed mode-I–II cracks in homogeneous isotropic unbounded media were considered. Attributed to the existence of the characteristic length in loading, it was long believed that the Wiener–Hopf technique could not be directly applied. Clever superpositions were then proposed by Freund (1974) and adopted by Brock (1982). In their analyses, the original problem was considered as a superposition of two of Lamb's problems and a superposition problem. The superposition problem concerned an unbounded solid containing a semi-infinite crack. Ahead of the crack tip, the solid was subjected to displacement discontinuities which were equal in magnitude but opposite in sign to the relative displacements of the two half-plane surfaces arising from Lamb's problems. Two of Lamb's problems and the superposition problem possessed no fixed characteristic length and were then solved by the Wiener–Hopf technique. Freund (1976) again investigated problem A in a review article as an illustration of the dynamic weighting function method.

In this article, we directly apply the Wiener–Hopf technique as if there were no characteristic length. The crucial steps in the analysis are integral transforms together with the direct application of Wiener–Hopf technique and Cagniard–de Hoop method. A summary of the Wiener–Hopf technique and Cagniard–de Hoop method can be found in Achenbach's book (1973). It is observed that the characteristic length in loading introduced an exponential term in the Wiener–Hopf equation. The sum splitting of the function, which exhibits an exponential behavior, is one of the most important steps in the analysis. This method of solution has potential with regard to the mixed mode-I–II crack problems with characteristic length in loading. It is fair to say that the superposition argument proposed by Freund (1974) offers better physical interpretation to the solution, while the current solution procedure is much more straightforward and more elegant.

It is of interest that the problem of mode-III crack propagation along the interface of two dissimilar isotropic half planes was considered by Brock and Achenbach (1973) where the crack was loaded by an anti-plane transient wave, and hence the problem contained no fixed characteristic length. The anti-plane response of a cracked homogeneous orthotropic strip was analyzed by Georgiadis (1986), who considered the steady-state crack problem and the characteristic length possessed in geometry but not in loading.

2. CORRESPONDENCE RELATION

Two-dimensional anti-plane wave motions of homogeneous, anisotropic, linearly-elastic solids are governed by (Crampin, 1981)

$$\hat{c}_{55}\frac{\partial^2\hat{w}}{\partial\hat{x}^2}+2\hat{c}_{45}\frac{\partial^2\hat{w}}{\partial\hat{x}\,\partial\hat{y}}+\hat{c}_{44}\frac{\partial^2\hat{w}}{\partial\hat{y}^2}=\hat{\rho}\frac{\partial^2\hat{w}}{\partial t^2} \tag{1}$$

where $\hat{w}(\hat{x},\hat{y},t)$ is the out-of-plane displacement, $\hat{c}_{ik}$ $(i,k=4,5)$ are elastic moduli and $\hat{\rho}$ is the mass density of the material. The $\hat{x}\hat{y}$-plane has been assumed to coincide with one of the planes of material symmetry, such that the in-plane and anti-plane motions are not coupled. The superposed hat indicates that the quantities are associated with the anisotropic solid. The relevant stress components are

$$\hat{\sigma}_{\hat{x}\hat{z}} = \hat{c}_{55}\frac{\partial \hat{w}}{\partial \hat{x}} + \hat{c}_{45}\frac{\partial \hat{w}}{\partial \hat{y}} \tag{2}$$

$$\hat{\sigma}_{\hat{y}\hat{z}} = \hat{c}_{45}\frac{\partial \hat{w}}{\partial \hat{x}} + \hat{c}_{44}\frac{\partial \hat{w}}{\partial \hat{y}}. \tag{3}$$

Introduce a coordinate transformation

$$x = \hat{x} - (\hat{c}_{45}/\hat{c}_{44})\hat{y} \tag{4}$$

$$y = (\mu/\hat{c}_{44})\hat{y} \tag{5}$$

$$z = \hat{z} \tag{6}$$

where $\mu = (\hat{c}_{44}\hat{c}_{55} - \hat{c}_{45}^2)^{1/2}$. The positiveness of $(\hat{c}_{44}\hat{c}_{55} - \hat{c}_{45}^2)$ is guaranteed by the positive definite of strain energy. Equations (4)–(6) and the chain rule of differentiation reduce (1) to the standard wave equation

$$\frac{\partial^2 \hat{w}}{\partial x^2} + \frac{\partial^2 \hat{w}}{\partial y^2} = s^2\frac{\partial^2 \hat{w}}{\partial y^2} \tag{7}$$

where $\rho = \hat{\rho}\hat{c}_{44}/\mu$ and

$$s^2 = \rho/\mu. \tag{8}$$

The constant $(\hat{c}_{44}/\mu)$ is the Jacobian of the coordinate transformation. Equation (7) suggests that it is possible to deduce the anti-plane shear solution for an anisotropic solid from a corresponding solution for an isotropic solid by a transformation of relevant parameters. The corresponding isotropic solid is characterized by the equivalent shear modulus μ and mass density ρ.

It is easily verified from (2)–(6) that the relevant displacement and stress components in a physical anisotropic solid are related to those in the corresponding isotropic solid by

$$\hat{w}(\hat{x}, \hat{y}, t) = w(x, y, t) \tag{9}$$

$$\hat{\sigma}_{\hat{x}\hat{z}}(\hat{x}, \hat{y}, t) = (\mu/\hat{c}_{44})\sigma_{xz}(x, y, t) + (\hat{c}_{45}/\hat{c}_{44})\sigma_{yz}(x, y, t) \tag{10}$$

$$\hat{\sigma}_{\hat{y}\hat{z}}(\hat{x}, \hat{y}, t) = \sigma_{yz}(x, y, t) \tag{11}$$

where the quantities without a superposed hat are associated with the corresponding isotropic solid, and $\sigma_{\alpha z} = \mu(\partial w/\partial \alpha)$, $\alpha = x, y$, are the relevant shear stresses. Under the transformation (4)–(6), straight lines making an angle $\hat{\theta}$ with the $\hat{x}$-axis in the $\hat{x}\hat{y}$-plane remain straight but make an angle θ with the x-axis in the xy-plane, where the angles $\hat{\theta}$ and θ are related by

$$\tan\hat{\theta} = \frac{(\hat{c}_{44}/\mu)\sin\theta}{\cos\theta + (\hat{c}_{45}/\mu)\sin\theta}, \tag{12}$$

while circles in the xy-plane correspond to ellipses in the $\hat{x}\hat{y}$-plane. In particular, the $\hat{x}$-axis is mapped onto the x-axis without any stretching; the y-axis is an axis which is orthogonal to the x-axis but not the mapping of the $\hat{y}$-axis. If a crack lies along the line $\hat{y} = 0$, $\hat{x} < 0$ in the $\hat{x}\hat{y}$-plane, it lies along the line $y = 0$, $x < 0$ in the xy-plane. Moreover, the mode-III stress intensity factors in both the physical and corresponding transformed coordinates are related by

$$\hat{K}_{III}(t) = K_{III}(t) \tag{13}$$

where the stress intensity factor $\hat{K}_{III}$ is defined as usual by

$$\hat{K}_{III}(t) = \lim_{\hat{x}\to 0^+} \sqrt{2\pi\hat{x}}\,\hat{\sigma}_{\hat{y}\hat{z}}(\hat{x}, 0, t) \tag{14}$$

and the definition of $K_{III}(t)$ is exactly the same as that of $\hat{K}_{III}(t)$ in (14), except that the quantities with a superposed hat are replaced by ones without hats. Hence if one can solve the problems of the corresponding isotropic solid, the solution for anti-plane shear problems involving an anisotropic solid can be obtained by appropriate substitution according to (9)–(11) and (13).

3. INTERFACE CRACK PROBLEM

Consider anti-plane deformations of a semi-infinite interface crack lying between dissimilar anisotropic half planes which are characterized by the elastic moduli $(\hat{c}_{ik})_j$, $i, k = 4, 5$, and mass densities $\hat{\rho}_j$. The subscript j ($j = 1, 2$) refers to the upper and lower media, respectively. Ahead of the crack tip the interface is perfectly welded. A Cartesian coordinate system is defined in such a way that the only nonzero displacement is normal to the $\hat{x}\hat{y}$-plane, and the crack lies in the line $\hat{y} = 0$, $\hat{x} < 0$. The materials are assumed to possess certain material symmetry and the $\hat{x}\hat{y}$-plane coincides with one of the planes of material symmetry, such that the in-plane and the anti-plane motions are not coupled. The crack geometry, the dissimilar anisotropic media and the coordinate system are shown in Fig. 1(a). Without loss of generality, one assumes that $\hat{s}_1 < \hat{s}_2$, where $\hat{s}_j = [\hat{\rho}\hat{c}_{44}/(\hat{c}_{44}\hat{c}_{55} - \hat{c}_{45}^2)]_j^{1/2}$ are the slownesses of the rays along the $\hat{x}$-direction in the upper and lower materials, respectively.

For time $t < 0$ the elastic solids are at rest. For time $t \geqslant 0$, a pair of concentrated anti-plane shear forces in the $\hat{z}$-direction of magnitudes F_1 and F_2 act on the crack faces $\hat{y} = 0^+$ and $\hat{y} = 0^-$, respectively, at $\hat{x} = -l$. Thus the crack-face boundary conditions are

$$\hat{\sigma}_{\hat{y}\hat{z}}(\hat{x}, \hat{y}, t) = \begin{cases} -F_1 H(t)\delta(\hat{x}+l), & \hat{x} < 0,\ \hat{y} = 0^+ \\ +F_2 H(t)\delta(\hat{x}+l), & \hat{x} < 0,\ \hat{y} = 0^- \end{cases} \tag{15}$$

where $H(\,)$ and $\delta(\,)$ are the Heaviside step and Dirac delta functions, respectively. Ahead of the crack tip, the interface boundary conditions which correspond to the continuity of displacement and traction along the welded part of the interface, along $\hat{x} > 0$, are

$$\hat{w}_1(\hat{x}, 0^+, t) = \hat{w}_2(\hat{x}, 0^-, t) \tag{16}$$

$$(\hat{\sigma}_{\hat{y}\hat{z}})_1(\hat{x}, 0^+, t) = (\hat{\sigma}_{\hat{y}\hat{z}})_2(\hat{x}, 0^-, t). \tag{17}$$

Notice that since the materials on both of the sides of the interface are different, the fields are no longer symmetric nor anti-symmetric with respect to $\hat{y} = 0$, even if the applied loadings are symmetric or anti-symmetric.

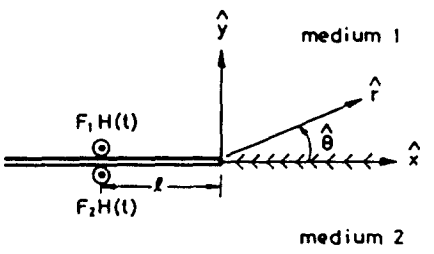

Fig. 1(a). Loading and crack geometry of the physical anisotropic bimaterial.

4. METHODS OF SOLUTION

The problem formulated in the previous section can be transformed into an isotropic one, and the transformations discussed in Section 2 apply. The coordinate transformation given by (4)–(6) maps the upper and lower anisotropic half planes onto their own corresponding isotropic half planes. As discussed in Section 2, the interface of a physical anisotropic bimaterial, the $\hat{x}$-axis, is mapped onto the interface of the corresponding isotropic bimaterial, the x-axis. Consequently, the corresponding problem concerns a semi-infinite interface crack lying along the line $y = 0$, $x < 0$, and between dissimilar isotropic half planes which are characterized by shear moduli $\mu_j \equiv [(\hat{c}_{44}\hat{c}_{55})_j - (\hat{c}_{45})_j^2]^{1/2}$ and mass densities $\rho_j \equiv (\hat{\rho}\hat{c}_{44}/\mu)_j$. The subscript j, $j = 1, 2$, refers to the upper and the lower media, respectively. The crack geometry, the corresponding dissimilar isotropic media and the transformed coordinate system as well as the wave pattern after the last wave has been diffracted are shown in Fig. 1(b). In this figure the direct waves produced by F_1 and F_2 are indicated by 1 and 2, respectively. The diffracted waves are indicated by two-digit numbers ij (i, $j = 1, 2$) which denote the waves in medium i resulting from the diffraction of a disturbance produced by applied force F_j.

From eqns (7) and (9), the anti-plane wave motions of the corresponding isotropic bimaterial in the transformed coordinates are governed by the standard wave equations

$$\frac{\partial^2 w_j}{\partial x^2} + \frac{\partial^2 w_j}{\partial y^2} = s_j^2 \frac{\partial^2 w_j}{\partial t^2}, \quad j = 1, 2 \tag{18}$$

where s is the slowness of the shear waves and is defined by (8). The relevant stress component is

$$(\sigma_{yz})_j = \mu_j \frac{\partial w_j}{\partial y}, \quad j = 1, 2. \tag{19}$$

It is easily verified that the assumption $\hat{s}_1 < \hat{s}_2$ implies $s_1 < s_2$. From (11) and (15)–(17), the crack-face boundary conditions in the xy-plane are

$$\sigma_{yz}(x, y, t) = \begin{cases} -F_1 H(t)\delta(x+l), & x < 0,\ y = 0^+ \\ +F_2 H(t)\delta(x+l), & x < 0,\ y = 0^-. \end{cases} \tag{20}$$

Ahead of the crack tip, the corresponding interface boundary conditions do not change along $x > 0$, except that the quantities with superposed hats are replaced by the ones without hats,

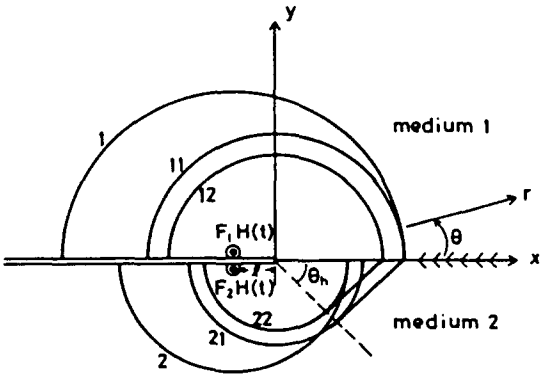

Fig. 1(b). Wave pattern of the corresponding isotropic problem.

$$w_1(x, 0^+, t) = w_2(x, 0^-, t) \tag{21}$$

$$(\sigma_{yz})_1(x, 0^+, t) = (\sigma_{yz})_2(x, 0^-, t). \tag{22}$$

Let us denote further the displacement and the traction along the welded part of the interface as $w_+(x, t)$ and $\sigma_+(x, t)$, respectively. The formulation given by (18)–(22) is formally identical to that for an interface crack lying between the isotropic bimaterial. The corresponding crack faces are loaded by a pair of concentrated anti-plane shear forces of magnitudes F_1 and F_2 at $(x, y) = (-l, 0^+)$ and $(-l, 0^-)$, respectively, for time $t \geq 0$. Hence the corresponding relations (9)–(14) can transform the solution of the isotropic interface crack problem into the anisotropic one formulated in Section 3.

Apply a one-sided Laplace transform over t, with kernel $\exp(-pt)$, and a two-sided Laplace transform over x, with kernel $\exp(-p\xi x)$, to the equation of motion (18). General solutions in the transformed domain, which are bounded as $y \to +\infty$ (and $-\infty$, respectively), can be written as

$$\tilde{\bar{w}}_1(\xi, y, p) = A \exp(-p\gamma_1 y), \quad y \geq 0 \tag{23}$$

$$\tilde{\bar{w}}_2(\xi, y, p) = B \exp(p\gamma_2 y), \quad y \leq 0 \tag{24}$$

where $\gamma_j^2 = (s_j^2 - \xi^2)$, $j = 1, 2$, and A and B are not-yet-determined arbitrary functions of ξ and p. The transformed function of one-sided and two-sided Laplace transforms are denoted by a superposed bar and tilde, respectively. The branch cuts of γ_j have been taken to be from $\xi \to -\infty$ to $-s_j$ and from $\xi = s_j$ to $\xi \to \infty$, $j = 1, 2$, such that $\mathrm{Re}(\gamma_j) \geq 0$ in the entire cut complex ξ-plane, where "Re" denotes the real part.

From (20), the transformed shear stresses along the whole crack line, $y = 0$, are

$$(\tilde{\bar{\sigma}}_{yz})_j(\xi, 0, p) = \tilde{\bar{\sigma}}_+ - \frac{\varepsilon F_j}{p} \exp(p\xi l), \quad j = 1, 2 \tag{25}$$

where $\tilde{\bar{\sigma}}_+$ is the transform of the unknown stress field, $\sigma_+(x, t)$, and the constant $\varepsilon = 1$ and -1 for medium 1 and 2, respectively. Because of the anticipated circular wavefronts and the existence of the head wavefront due to the mismatched bimaterial, the wave fields along $y = 0$ are zero beyond $|x - l| = t/s_1$. By virtue of the theory of Laplace transform, both $\tilde{\bar{\sigma}}_+$ and $\tilde{\bar{w}}_+$ are analytic and go to zero as $|\xi| \to +\infty$ in the half complex ξ-plane $\mathrm{Re}(\xi) > -s_1$, where $\tilde{\bar{w}}_+$ is the transformed unknown displacement $w_+(x, t)$.

From (23)–(24), the transformed displacements of media 1 and 2 along the crack line are

$$\tilde{\bar{w}}_{1-} + \tilde{\bar{w}}_+ = A, \quad y = 0^+ \tag{26}$$

$$\tilde{\bar{w}}_{2-} + \tilde{\bar{w}}_+ = B, \quad y = 0^- \tag{27}$$

and the transformed shear stresses along the crack line are

$$\tilde{\bar{\sigma}}_+ - \frac{F_1}{p} \exp(p\xi l) = -p\mu_1\gamma_1 A, \quad y = 0^+ \tag{28}$$

$$\tilde{\bar{\sigma}}_+ + \frac{F_2}{p} \exp(p\xi l) = p\mu_2\gamma_2 B, \quad y = 0^-. \tag{29}$$

In (26) and (27), $\tilde{\bar{w}}_{1-}$ and $\tilde{\bar{w}}_{2-}$ are transforms of the unknown crack-face displacements, $w_{1-}(x, t)$, $w_{2-}(x, t)$, of the upper and lower crack faces, respectively. Notice that w_{j-} ($j = 1, 2$) vanishes for $x > 0$, and moreover, because of anticipated circular wavefronts, w_{j-} also vanishes for $x < -t/s_j - l$. By virtue of the theory of Laplace transform, $\tilde{\bar{w}}_{1-}$ and $\tilde{\bar{w}}_{2-}$ are

analytic and go to zero as $|\xi| \to \infty$ in the half complex ξ-planes $\mathrm{Re}(\xi) < s_j$, respectively. Relating transformed crack-line stresses and displacements through (26)–(29), eliminating $\tilde{\bar{w}}_+$, and defining $\tilde{\bar{w}}_- \equiv \tilde{\bar{w}}_{1-} - \tilde{\bar{w}}_{2-}$ which denotes the transformed crack-opening displacement, one has

$$\tilde{\bar{w}}_- = -\frac{1}{p}\Gamma(\xi)\tilde{\bar{\sigma}}_+ + \frac{1}{p^2}\left(\frac{F_1}{\mu_1\gamma_1} - \frac{F_2}{\mu_2\gamma_2}\right)\exp(p\xi l) \tag{30}$$

where

$$\Gamma(\xi) = \frac{\mu_1\gamma_1 + \mu_2\gamma_2}{\mu_1\mu_2\gamma_1\gamma_2}. \tag{31}$$

5. WIENER-HOPF TECHNIQUE

Equation (30) has been cast into a form suitable for the application of the Wiener–Hopf technique. Introduce a new function $\Gamma^*(\xi)$ by defining

$$\Gamma^*(\xi) = \frac{\gamma_1}{\kappa}\Gamma(\xi) \tag{32}$$

where $\kappa = (\mu_1+\mu_2)/(\mu_1\mu_2)$. The function $\Gamma^*(\xi) \to 1$ as $|\xi| \to \infty$, moreover, has neither zero nor pole, and is single-valued in the entire complex ξ-plane by cuts along $-s_2 < \xi < -s_1$ and $s_1 < \xi < s_2$. From the analytic function theory, therefore, Γ^* can be written as the product of two regular functions Γ^*_+ and Γ^*_-. By directly applying the formula of sum splitting (Noble, 1958) to $\ln \Gamma^*(\xi)$, replacing the original contour of integration by finite contours wrapped around the lower and upper faces of an appropriate branch cut, and then taking the exponential, one has

$$\Gamma^*_\pm(\xi) = \exp\left\{-\frac{1}{\pi}\int_{s_1}^{s_2} \tan^{-1}\left[\frac{\mu_1(\eta^2-s_1^2)^{1/2}}{\mu_2(s_2^2-\eta^2)^{1/2}}\right]\frac{1}{\eta \pm \xi}\,\mathrm{d}\eta\right\}. \tag{33}$$

Notice that the functions $\Gamma^*_+(\xi)$ and $\Gamma^*_-(\xi)$ are regular at every point in the half planes $\mathrm{Re}(\xi) > -s_1$ and $\mathrm{Re}(\xi) < s_1$, respectively. Moreover, $\Gamma^*_+(\xi)$ $[\Gamma^*_-(\xi)]$ has a branch cut along $-s_2 < \xi < -s_1$ $(s_1 < \xi < s_2)$ as $\Gamma^*(\xi)$ in the left (right) half of the ξ-plane. It is of interest that the quotient splitting of $\Gamma(\xi)$ was also studied by Ament (1954) using a complicated change of variable and followed by a simple inspection.

Equation (30) can then be arranged in the form

$$\frac{\gamma_{1-}}{\Gamma^*_-}\tilde{\bar{w}}_- = -\frac{\kappa}{p}\frac{\Gamma^*_+}{\gamma_{1+}}\tilde{\bar{\sigma}}_+ + \frac{1}{p^2}D(\xi) \tag{34}$$

where $\gamma_{1\pm} = (s_1 \pm \xi)^{1/2}$, and

$$D(\xi) = \frac{\gamma_{1-}}{\Gamma^*_-}\left(\frac{F_1}{\mu_1\gamma_1} - \frac{F_2}{\mu_2\gamma_2}\right)\exp(p\xi l). \tag{35}$$

Since the function $D(\xi)$ is analytic and goes to zero as $|\xi| \to \infty$ in the strip $-s_1 < \mathrm{Re}(\xi) < s_1$, it can be expressed as the sum of the two functions $D_+(\xi)$ and $D_-(\xi)$, and the formula of sum splitting directly applies

$$D_+(\xi) = \int_{s_1}^{\infty} \frac{G_1(\eta)}{(\eta+\xi)} e^{-p\eta l} d\eta - \int_{s_2}^{\infty} \frac{G_2(\eta)}{(\eta+\xi)} e^{-p\eta l} d\eta \tag{36}$$

$$D_-(\xi) = D(\xi) - D_+(\xi) \tag{37}$$

where

$$G_1(\eta) = \frac{1}{\pi} \frac{F_1}{\mu_1} \frac{1}{(\eta - s_1)^{1/2} \Gamma_+^*(\eta)} \tag{38}$$

$$G_2(\eta) = \frac{1}{\pi} \frac{F_2}{\mu_2} \frac{(s_1+\eta)^{1/2}}{(\eta^2 - s_2^2)^{1/2} \Gamma_+^*(\eta)}. \tag{39}$$

Functions $D_+(\xi)$ and $D_-(\xi)$ are regular at every point in the half complex ξ-planes of $\mathrm{Re}(\xi) > -s_1$ and $\mathrm{Re}(\xi) < s_1$, respectively.

Equation (34) now becomes

$$\frac{\gamma_{1-}}{\Gamma_-^*} \tilde{w}_- - \frac{1}{p^2} D_-(\xi) = -\frac{\kappa}{p} \frac{\Gamma_+^*}{\gamma_{1+}} \tilde{\sigma}_+ + \frac{1}{p^2} D_+(\xi). \tag{40}$$

The left-hand and right-hand sides of (40) are clearly regular in the overlapping half planes $\mathrm{Re}(\xi) < s_1$ and $\mathrm{Re}(\xi) > -s_1$, respectively. By analytic continuation, therefore, each side of (40) is the unique analytic continuation of the other into the complementary half plane, and both sides represent one and the same entire function, say Z. Liouville's theorem for bounded entire functions allows the conclusion $Z \equiv$ constant. The magnitude of the constant can be obtained from order conditions on Z as $|\xi| \to \infty$, which in turn are obtained from order conditions on the dependent field variables in the vicinity of $x = 0$. As usual, the near-tip stress fields and the crack-opening displacement exhibit inverse square root and square root behaviors, respectively, with the result that Z vanishes completely, hence

$$\tilde{\sigma}_+(\xi, 0, p) = \frac{1}{p} \frac{1}{\kappa} \frac{\gamma_{1+}(\xi)}{\Gamma_+^*(\xi)} D_+(\xi). \tag{41}$$

The transformed crack-line stresses are thus completely determined.

It is worthwhile mentioning that in the cases of anti-symmetric loading, $F_1 = -F_2 \equiv F$, the function $D(\xi)$ is simplified to $D_a(\xi)$ as

$$D_a(\xi) = \frac{F\kappa\Gamma_+^*(\xi)}{\gamma_{1+}(\xi)} \exp(p\xi l). \tag{42}$$

Through careful studies on the behaviors of the functions γ_{1+} and Γ_+^*, it has been concluded that $D_a(\xi)$ has a branch cut along $-\infty < \xi < -s_1$ only. Since $\exp(p\xi l)$ is an entire function in the whole complex ξ-plane, $D_a(\xi)$ is then analytic in the half plane $\mathrm{Re}(\xi) > -s_1$. The left-hand and the right-hand sides of (34) are then analytic in the overlapping half planes $\mathrm{Re}(\xi) < s_1$ and $\mathrm{Re}(\xi) > -s_1$. Hence both sides represent one and the same entire function and it might appear that our problem has been solved. Unfortunately, the function $D_a(\xi)$ is not bounded as $\mathrm{Re}(\xi) \to \infty$ owing to the presence of the exponential term $\exp(p\xi l)$. This prevents one from determining the entire function. Hence a sum splitting for $D_a(\xi)$ into two regular functions, D_{a+} and D_{a-}, in appropriate complex half planes is still necessary. The results for D_{a+} and D_{a-} can be directly deduced from (36)–(39) by letting $F_1 = -F_2 \equiv F$.

6. STRESS INTENSITY FACTOR

Stress intensity factors can now be concluded. Inverting the two-sided Laplace transform to (41) and changing the order of integration between the integrals over the transformed variable ξ and that in $D_+(\xi)$, one has

$$\bar{\sigma}_+(x,0,p) = \int_{s_1}^{\infty} G_1(\eta)\bar{I}(\eta,p)\,d\eta - \int_{s_2}^{\infty} G_2(\eta)\bar{I}(\eta,p)\,d\eta \tag{43}$$

where

$$\bar{I}(\eta,p) = \frac{1}{2\pi i}\int_{Br} \frac{\gamma_{1+}(\xi)}{\kappa\Gamma_+^*(\xi)} \frac{\exp[-p(\eta l-\xi x)]}{(\eta+\xi)}\,d\xi \tag{44}$$

and Br is the Bromwich contour of the inverse transform. The functions $G_1(\eta)$ and $G_2(\eta)$, defined in (38) and (39), are contributions from F_1 and F_2, respectively. For $x > 0$, the path Br is deformed to wrap around the lower and upper faces of the branch cut $\xi < -s_1$. No singularities of the integrand are crossed in the process, and the integrand meets the conditions of Jordan's lemma. After some manipulations it yields, for $x > 0$,

$$\bar{I}(\eta,p) = \frac{1}{\pi\kappa}\int_{s_1}^{\infty} \mathrm{Re}\left[\frac{1}{\Gamma_-^*(\xi)}\right]\frac{(\xi-s_1)^{1/2}}{(\xi-\eta)}\exp[-p(\eta l+\xi x)]\,d\xi$$
$$+\frac{1}{\kappa}H(\eta-s_1)H(s_2-\eta)\mathrm{Re}\left[\frac{\gamma_{1-}(\eta)}{\Gamma_-^*(\eta)}\right]\exp[-p\eta(l+x)]. \tag{45}$$

By the Cagniard–de Hoop method, letting $\eta l+\xi x = t$ and inverting the one-sided Laplace transform by inspection, one has

$$I(\eta,t) = \frac{1}{\pi\kappa}H(t-\eta l-s_1x)\,\mathrm{Re}\left[\frac{1}{\Gamma_-^*\left(\dfrac{t-\eta l}{x}\right)}\right]\frac{(t-\eta l-s_1x)^{1/2}}{x^{1/2}(t-\eta l-\eta x)}$$
$$+\frac{1}{\kappa}H(\eta-s_1)H(s_2-\eta)\mathrm{Re}\left[\frac{\gamma_{1-}(\eta)}{\Gamma_-^*(\eta)}\right]\delta(t-\eta l-\eta x). \tag{46}$$

Concluding from (14), (43) and (46) yields the resulting mode-III stress intensity factor as

$$\hat{K}_{III}(t) = \sqrt{\frac{2}{\pi l}}\frac{1}{\kappa}\cdot\left\{H(t-s_1l)\int_{s_1}^{t/l}\frac{G_1(\eta)}{(t/l-\eta)^{1/2}}\,d\eta - H(t-s_2l)\int_{s_2}^{t/l}\frac{G_2(\eta)}{(t/l-\eta)^{1/2}}\,d\eta\right\}. \tag{47}$$

It is of interest to discuss two special cases. For the cases of anti-symmetric loadings ($F_1 = -F_2 \equiv F$), the stress intensity factors (47) can be simplified as

$$\hat{K}_{III}(t) = H(t-s_1l)\sqrt{\frac{2}{\pi l}}\frac{F}{\pi}\int_{s_1}^{t/l}\frac{\mathrm{Re}[\Gamma_-^*(\eta)]}{(t/l-\eta)^{1/2}(\eta-s_1)^{1/2}}\,d\eta. \tag{48}$$

Notice that for time $t > s_2l$, (48) can be evaluated analytically by complex integration in the η-plane. In this case, the integral in (48) is equal to the integral taken along a closed contour of infinitely large radius by using Cauchy's theorem. The final result for $t > s_2l$ is

$$\hat{K}_{III}(t) = \sqrt{\frac{2}{\pi l}} F. \tag{49}$$

Equation (49) is exactly the appropriate static result for a pair of concentrated forces applied to interface cracks in bimaterials as well as to cracks in homogeneous media.

In the cases where $s_1 = s_2 \equiv s$, the functions $\Gamma(\xi)$ and $D_+(\xi)$ are simplified to

$$\Gamma(\xi) = \kappa (s^2 - \xi^2)^{1/2} \tag{50}$$

$$D_+(\xi) = \frac{1}{\pi}\left(\frac{F_1}{\mu_1} - \frac{F_2}{\mu_2}\right) \int_s^\infty \frac{\exp(-p\eta l)}{(\eta+\xi)(\eta-s)^{1/2}} \, d\eta. \tag{51}$$

The stress intensity factor jumps immediately from zero to the appropriate static result for an interface crack in a bimaterial, once waves arrive on the crack tip

$$\hat{K}_{III}(t) = \sqrt{\frac{2}{\pi l}} \frac{1}{\kappa}\left(\frac{F_1}{\mu_1} - \frac{F_2}{\mu_2}\right) H(t - sl). \tag{52}$$

7. RADIATION FIELDS

The transformed radiation stress fields are concluded from (19), (23)–(24), (28)–(29) and (41) to be

$$\begin{Bmatrix} (\tilde{\sigma}_{yz})_j \\ (\tilde{\sigma}_{xz})_j \end{Bmatrix} = \begin{Bmatrix} g_{yj}(\xi) \\ g_{xj}(\xi) \end{Bmatrix} E_j(\xi, p) \exp(-p\gamma_j |y|) \tag{53}$$

where

$$E_j(\xi, p) = \frac{1}{p}\left[\frac{1}{\kappa} \frac{\gamma_{1+}(\xi) D_+(\xi)}{\Gamma_+^*(\xi)} - \varepsilon F_j e^{p s l}\right] \tag{54}$$

$$\begin{Bmatrix} g_{yj}(\xi) \\ g_{xj}(\xi) \end{Bmatrix} = \begin{Bmatrix} 1 \\ -\varepsilon\xi/(s_j^2 - \xi^2)^{1/2} \end{Bmatrix} \tag{55}$$

and the subscript j ($j = 1, 2$) refers to medium 1 ($y \geqslant 0$, $\varepsilon = +1$) and medium 2 ($y \leqslant 0$, $\varepsilon = -1$), respectively.

The stress fields in the (x, y, t) domain can be found by the direct application of the Cagniard–de Hoop method. The Cauchy theorem is used to deform the original integration paths of inverse transforms to Cagniard paths. The results yield

$$(\sigma_{\alpha z})_j^c(x, y, t) = h_{\alpha j} H(t - s_j R) + H(t - t_{aj}) \int_{s_1}^{s_{cj}} G_1(\eta) G_{\alpha j}^c(\eta) \, d\eta - H(t - t_{bj}) \int_{s_2}^{s_{cj}} G_2(\eta) G_{\alpha j}^c(\eta) \, d\eta, \quad \alpha = x, y \tag{56}$$

where the superscript c stands for the contribution of the Cagniard path, and the upper limit of the integration is

$$s_{cj} = (t - s_j r)/l. \tag{57}$$

The arrival times t_{aj} and t_{bj} are defined as $t_{aj} = s_1 l + s_j r$ and $t_{bj} = s_2 l + s_j r$, respectively. The expressions for $G_{\alpha j}^c$ and $h_{\alpha j}$ are

$$G_{xj}^{c}(\eta) = \frac{1}{\pi} \operatorname{Im}\left[\frac{g_{xj}(\xi)\gamma_{1+}(\xi)}{\kappa(\eta+\xi)\Gamma_{+}^{*}(\xi)} \frac{\partial \xi_{cj}}{\partial t}\right]\Bigg|_{\xi=\xi_{cj}} \tag{58}$$

$$\begin{Bmatrix} h_{yj} \\ h_{xj} \end{Bmatrix} = -\frac{F_j}{\pi} \frac{1}{R} \frac{t}{\sqrt{t^2-(s_j R)^2}} \begin{Bmatrix} \sin\phi \\ \cos\phi \end{Bmatrix} \tag{59}$$

where "Im" denotes the imaginary part, and the variable ξ_{cj} in (58) is a function of η given by

$$\xi_{cj} = \frac{1}{r}\{-(t-\eta l)\cos\theta + \mathrm{i}\,|\sin\theta|\,[(t-\eta l)^2 - s_j^2 r^2]^{1/2}\}. \tag{60}$$

Here $r \equiv (x^2+y^2)^{1/2}$, $\theta \equiv \tan^{-1}(y/x)$ are polar coordinates centered at $(x, y) = (0, 0)$; while $R \equiv [(x+l)^2+y^2]^{1/2}$, $\phi \equiv \tan^{-1}[y/(x+l)]$ centered at $(x, y) = (-l, 0^{\pm})$. From the viewpoint of wave propagation, the first term in (56) defines cylindrical waves which radiate from $(x, y) = (-l, 0^{\pm})$. It is identified as the solution of Lamb's problem with concentrated force F_j acting on the free surface of half plane j at $(x, y) = (-l, 0)$. The integrals in (56) define cylindrical waves which radiate from the crack tip and are contributions from the applied forces F_1 and F_2, respectively, at $(x, y) = (-l, 0^{\pm})$. The Heaviside functions in eqn (56) clearly indicate that these cylindrical wavefronts are circles, while they are ellipses in the physical anisotropic bimaterial due to the corresponding relations discussed in Section 2.

For medium 2, $y \leqslant 0$, it is possible that the Cagniard path intersects, and therefore must be deformed around, the branch cut. Moreover, the branch line integral encloses a simple pole. The branch line integral and the residual of the pole give extra contributions. The regions influenced by these contributions are $-\cos^{-1}(s_1/s_2) < \theta \leqslant 0$. The residual only contributes to F_1 and is expressed as

$$(\sigma_{xz})_2^{\mathrm{p}}(x, y, t) = \frac{F_1}{\pi} H(s_2\cos\theta - s_1) H(t-t_{\mathrm{p}1}) H(t_{\mathrm{p}2}-t) G_{x2}^{\mathrm{p}}(\xi_{\mathrm{p}}) \frac{\partial \xi_{\mathrm{p}}}{\partial t} \tag{61}$$

where

$$G_{x2}^{\mathrm{p}}(\xi) \equiv g_{x2}(-\xi) \frac{\mu_1\mu_2|\gamma_1|\gamma_2}{(\mu_1|\gamma_1|)^2+(\mu_2\gamma_2)^2} \tag{62}$$

$$\xi_{\mathrm{p}} = [t\cos\phi - (s_2^2R^2 - t^2)^{1/2}|\sin\phi|]/R. \tag{63}$$

The starting and ending times of the pole contribution are defined as

$$t_{\mathrm{p}1} = s_1(x+l) - (s_2^2-s_1^2)^{1/2} y \tag{64}$$

$$t_{\mathrm{p}2} = s_2(r+l\cos\theta). \tag{65}$$

The contributions from the branch line integral are

$$(\sigma_{xz})_2^{\mathrm{h}}(x, y, t) = H(s_2\cos\theta - s_1)\left\{H(t-t_{\mathrm{h}1})\int_{s_{\mathrm{h}1}}^{s_{\mathrm{h}3}} G_1(\eta) G_{x2}^{\mathrm{h}}(\eta)\,\mathrm{d}\eta - H(t-t_{\mathrm{h}2})\int_{s_{\mathrm{h}2}}^{s_{\mathrm{h}3}} G_2(\eta) G_{x2}^{\mathrm{h}}(\eta)\,\mathrm{d}\eta\right\} \tag{66}$$

where

$$G^{h}_{xz}(\eta) = \frac{1}{\pi\kappa}\frac{g_{xz}(-\xi_h)(\xi_h - s_1)^{1/2}}{(\xi_h - \eta)}\,\mathrm{Re}\left[\frac{1}{\Gamma^{*}_{-}(\xi_h)}\right]\frac{\partial\xi_h}{\partial t} \tag{67}$$

$$\xi_h = \frac{1}{r}\{(t-\eta l)\cos\theta - [s_2^2 r^2 - (t-\eta l)^2]^{1/2}|\sin\theta|\}. \tag{68}$$

The integration limits in (66) are defined as

$$s_{hj} = \max(s_j, s_{c2}), \quad j = 1, 2 \tag{69}$$

$$s_{h3} = [t - s_1 x + (s_2^2 - s_1^2)^{1/2} y]/l. \tag{70}$$

The arrival times are $t_{h1} = t_{p1}$, and $t_{h2} = s_1 x + s_2 l - (s_2^2 - s_1^2)^{1/2} y$. Notice that $(\xi_h - \eta)$ goes to zero for a particular η between s_{h1} and s_{h3}, and the first integral in (66) is in the sense of the Cauchy principal value. From the viewpoint of wave propagation (61) and (66) describe head waves generated by the mismatched bimaterial.

Detailed asymptotic analyses show that stress components $\sigma_{\alpha z}$ ($\alpha = x$ and y) possess inverse square root behaviors near wavefronts of the direct waves, i.e. near $t = s_j R$, while they are continuous at $t = t_{h2}$ and t_{p1} but possess finite jumps at the rest of the wavefronts. In the head wave region, the logarithmic behaviors' contribution to the branch line integrals covers up the finite discontinuities at $t = t_{a2}$ and t_{b2}. Hence the radiated stress fields in medium 1 first experience an inverse square root behavior at $t = s_1 R$ followed by two finite jumps T^{a}_{a1} and T^{a}_{b1} at $t = t_{a1}$ and t_{b1}, respectively. The radiated stress fields in medium 2 are slightly complicated. Outside the head region, they first experience three jumps at $t = t_{h1}$, t_{a2} and t_{p2} followed by an inverse square root behavior and a finite discontinuity at $t = s_2 R$ and t_{b2}, respectively, whereas for the head region, the logarithmic behaviors at $t = t_{a2}$ and t_{b2}, rather than the discontinuities, are dominant. The constants $T^{\alpha}_{\beta j}$ ($\alpha = x, y$; $\beta = a, b$, p, h, and $j = 1, 2$), which denote the amount of discontinuities in stress components $\sigma_{\alpha z}$ at time $t = t_{\beta j}$, are defined as

$$T^{\alpha}_{aj} = \frac{F_1}{\mu_1}\frac{1}{\Gamma^{*}_{+}(s_1)}B_{\alpha j} \tag{71}$$

$$T^{\alpha}_{bj} = \frac{F_2}{\mu_2}\frac{1}{\Gamma^{*}_{+}(s_2)}\frac{(s_1+s_2)^{1/2}}{(2s_2)^{1/2}}B_{\alpha j} \tag{72}$$

$$T^{\alpha}_{p2} = \frac{F_1\mu_1}{\pi l\mu_2}\frac{(s_2^2\cos^2\theta - s_1^2)^{1/2}}{s_2|\sin\theta|}g_{xz}(-s_2\cos\theta) \tag{73}$$

$$T^{\alpha}_{h1} = \frac{F_1 l^{1/2}}{\pi}\left(\frac{\partial\xi_h}{\partial t}\right)^{3/2}\frac{1}{\left(l\dfrac{\partial\xi^h}{\partial t}+1\right)}g_{xz}(-s_1) \tag{74}$$

where

$$B_{\alpha j} = \frac{1}{\pi(2ls_j r)^{1/2}}\mathrm{Re}\left[\frac{g_{\alpha j}(\xi)\gamma_{1+}(\xi)\gamma_j(\xi)}{\kappa(s_1+\xi)\Gamma^{*}_{+}(\xi)}\right]\Bigg|_{\xi=-s_j\cos\theta} \tag{75}$$

$$\frac{\partial\xi_h}{\partial t} = \frac{1}{r}\frac{(s_2^2 - s_1^2)^{1/2}}{(s_2^2 - s_1^2)^{1/2}\cos\theta + s_1\sin\theta}. \tag{76}$$

It is of interest to consider the stress components in polar coordinates. The time history of $\sigma_{\theta z}$ is quite different from those of the other stress components. In medium 1, the transient

response of $\sigma_{\theta z}$ experiences only an inverse square root behavior at $t = s_1 R$ and then is continuous elsewhere. The cancellation of the jump contributions from σ_{xz} and σ_{yz} is owing to the terms g_{xj} in the expressions for B_{xj}, $\alpha = x, y$. Similarly, $\sigma_{\theta z}$ in medium 2 experiences jumps only at $t = t_{h1}$ and t_{p2} and an inverse square root behavior at $s_1 R$ but is continuous elsewhere.

8. RESULTS

There are numerous parameters in the present analysis. They may be subdivided into material parameters, a geometric parameter, and loading parameters. The material parameters are the mass density $\hat{\rho}_j$, and the shear moduli $(\hat{c}_{ik})_j$ $(i, k = 4, 5)$ of upper and lower materials $(j = 1, 2)$. The geometric parameter is the characteristic length l. The loading parameters are the magnitudes of applied forces F_1 and F_2.

The elastodynamic mode-III stress intensity factors of an interface crack in an anisotropic bimaterial as defined by (13) and (47) depend on material parameters only for the ratio of equivalent slownesses s_2/s_1, and the ratio of equivalent shear moduli μ_2/μ_1. Figures 2–6 show the dimensionless stress intensity factors versus dimensionless time for various values of s_2/s_1 and μ_2/μ_1. For $s_2/s_1 = 10$ with anti-symmetric loadings $(F_1 = -F_2 \equiv F)$, Fig. 2 shows K_{III}/K_a as a function of $t/(s_1 l)$ for various values of μ_2/μ_1, where $K_a = (2/\pi l)^{1/2} F$ is the appropriate static value. It is noted that the stress intensity factors are almost constants

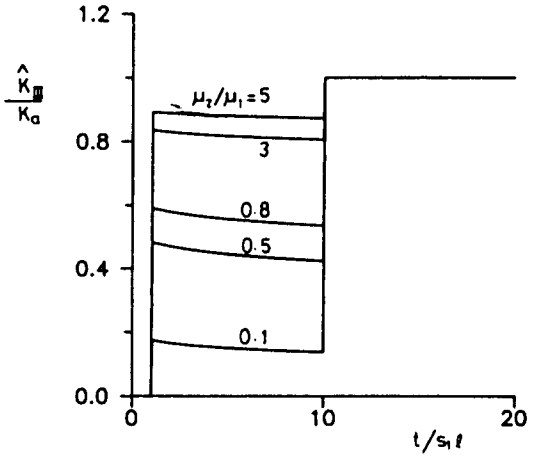

Fig. 2. Mode-III stress intensity factor for anti-symmetric loading $(F_1 = -F_2 \equiv F)$ and $s_2/s_1 = 10$.

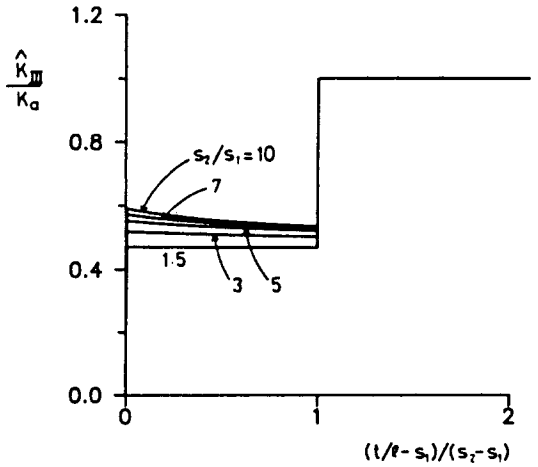

Fig. 3. Mode-III stress intensity factor for anti-symmetric loading $(F_1 = -F_2 \equiv F)$ and $\mu_2/\mu_1 = 0.8$.

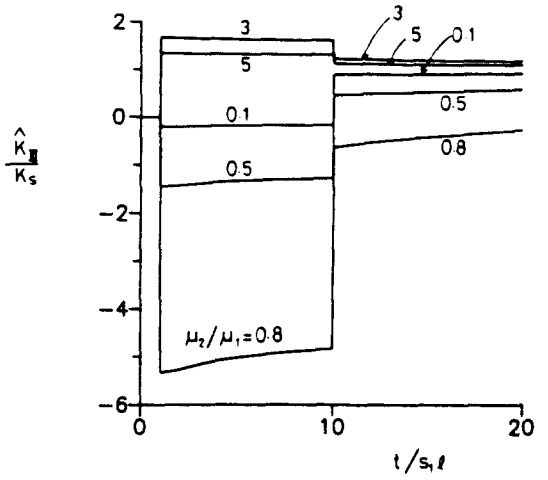

Fig. 4. Mode-III stress intensity factor for symmetric loading ($F_1 = F_2 \equiv F$) and $s_2/s_1 = 10$.

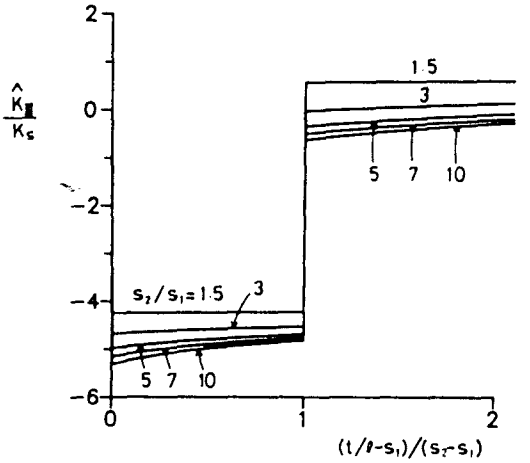

Fig. 5. Mode-III stress intensity factor for symmetric loading ($F_1 = F_2 \equiv F$) and $\mu_2/\mu_1 = 0.8$.

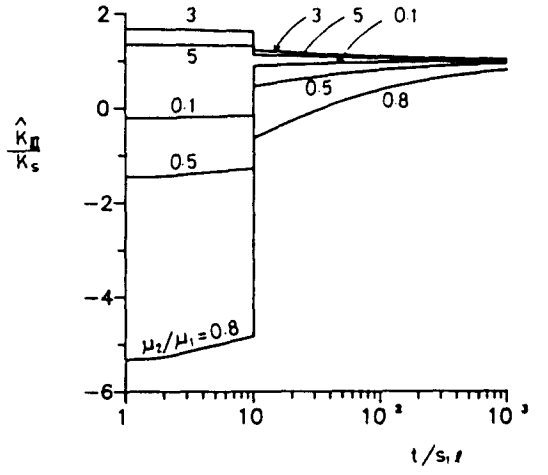

Fig. 6. Mode-III stress intensity factor for symmetric loading ($F_1 = F_2 \equiv F$) and $s_2/s_1 = 10$ versus logarithmic scale of dimensionless time.

with respect to the variation of t, and jump to the static value immediately at $t = s_2 l$. Moreover, for $t < s_2 l$ the larger μ_2/μ_1 is, the closer the stress intensity factor to the static value. On the other hand, the smaller μ_2/μ_1 is, the smaller the stress intensity factor for $t < s_2 l$. These are as one would expect. In fact, in the limiting case of $\mu_2/\mu_1 \to \infty$ one would expect that the solution in medium 1 for $t < s_2 l$ is almost the same as the solution for a semi-infinite crack in a homogeneous unbounded domain (with only medium 1) subjected to anti-symmetric loading, while in the case of $\mu_2/\mu_1 \to 0$ one would expect the solution to be that of a semi-infinite crack in a homogeneous unbounded domain subjected to the symmetric loading. For $\mu_2/\mu_1 = 0.8$, Fig. 3 shows $\hat{K}_{III}/K_a$ as a function of $(t/l - s_1)/(s_2 - s_1)$ for various values of s_2/s_1. It is of interest to point out that for the cases of $s_2/s_1 = 1$, $\hat{K}_{III}$ jumps immediately to K_a at $t = s_1 l$ as discussed in Section 6. This result cannot be included in Fig. 3 due to the abscissa of the figure.

The analogous curves for symmetric loadings ($F_1 = F_2 \equiv F$) are shown in Figs 4–5, except that $\hat{K}_{III}$ is now dimensionless by the appropriate static value K_s, where

$$K_s = (2/\pi l)^{1/2}(\mu_2 - \mu_1)/(\mu_2 + \mu_1). \tag{77}$$

Since $K_s = 0$ as $\mu_2/\mu_1 = 1$, the dimensionless $\hat{K}_{III}$ for the case where $\mu_2/\mu_1 \to 1$ is magnified by larger factors than other cases. The variation of the history of $\hat{K}_{III}$ is very similar to that for the case of anti-symmetric loading, except that the stress intensity factors now approach the static values quite slowly, especially for $\mu_2/\mu_1 \to 1$. The semi-logarithmic plot of $\hat{K}_{III}/K_s$ versus the logarithmic scale of $t/(s_1 l)$ is shown in Fig. 6. It is noted that $\hat{K}_{III}$ approaches only 85% of the static value for the case $\mu_2/\mu_1 = 0.5$ even when $t/(s_1 l) = 100$. It is also of interest to point out that the stress intensity factors completely vanish only if the upper and lower materials are identical.

The radiated stress fields in an isotropic bimaterial are the sum of (56), (61) and (66). Those of the anisotropic bimaterial are then deduced from (10)–(11), and their polar components are obtained accordingly. The time history of $\hat{\sigma}_{\hat{\theta}\hat{z}}$ has fewer discontinuities and fewer logarithmic singularities than those of $\hat{\sigma}_{\hat{x}\hat{z}}$, $\hat{\sigma}_{\hat{y}\hat{z}}$ and $\hat{\sigma}_{\hat{r}\hat{z}}$ as discussed in the previous section for the corresponding isotropic bimaterial. The influenced region of the head waves in the anisotropic bimaterial is $\hat{\theta}_h < \hat{\theta} < 0$, where $(\hat{r}, \hat{\theta})$ are the polar coordinates in the $\hat{x}\hat{y}$-plane. The angle $\hat{\theta}_h$ is defined as $\hat{\psi}$ and $-(\pi - \hat{\psi})$ for $s_1 - (\hat{c}_{45}/\mu)_2(s_2^2 - s_1^2)^{1/2} \geqslant 0$ and < 0, respectively, where from (12)

$$\hat{\psi} = \tan^{-1}\left[\frac{-(\hat{c}_{44}/\mu)_2(s_2^2 - s_1^2)^{1/2}}{s_1 - (\hat{c}_{45}/\mu)_2(s_2^2 - s_1^2)^{1/2}}\right]. \tag{78}$$

Numerical calculations have been carried out for various values of $\hat{r}/l$ and angle $\hat{\theta}$ for both the cases of anti-symmetric and symmetric loadings. Only some typical results are presented in the paper. As fixed parameters, we have chosen a carbon–epoxy composite and a graphite–epoxy composite as media 1 and 2, respectively. Typical material properties are $\hat{\rho} = 1.57 \times 10^3$ kg m^{-3}, $\hat{c}_{44} = 3.98$ Gpa, $\hat{c}_{55} = 6.4$ Gpa, $\hat{c}_{45} = 0$, for carbon–epoxy and $\hat{\rho} = 1.6 \times 10^3$ kg m^{-3}, $\hat{c}_{44} = 6.55$ Gpa, $\hat{c}_{55} = 2.6$ Gpa, $\hat{c}_{45} = 0$, for graphite–epoxy. Figures 7–10 show the dimensionless radiated stress fields versus dimensionless time. Since the order of magnitude of $\hat{\sigma}_{\hat{\theta}\hat{z}}$ is less than that of $\hat{\sigma}_{\hat{r}\hat{z}}$ by one, double ordinate plots are used to incorporate both components in the same figure. Figure 7 shows $\hat{\sigma}_{\hat{r}\hat{z}}/F$ and $\hat{\sigma}_{\hat{\theta}\hat{z}}/F$ as functions of $t/(s_1 l)$ at $\hat{r}/l = 1$ and $\hat{\theta} = |\hat{\theta}_h|/2$, i.e. in medium 1, for anti-symmetric loadings. The analogous curves for $\hat{r}/l = 1$, $\hat{\theta} = \hat{\theta}_h/2$, i.e. in medium 2, are shown in Fig. 8. It is noted that time histories of the radiated stress fields in medium 1 have less jumps than those in the head wave region of medium 2. Moreover, jumps are consistent with the wavefront analyses in the last section. The analogous curves for the cases of symmetric loadings at positions $\hat{r}/l = 1$, $\hat{\theta} = |\hat{\theta}_h|/2$ and $\hat{\theta}_h/2$, are shown in Figs 9–10, respectively.

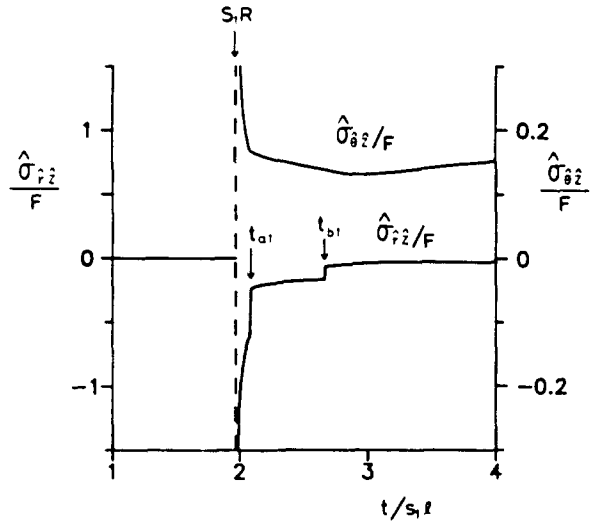

Fig. 7. Radiated stress history for anti-symmetric loading ($F_1 = -F_2 \equiv F$) at $\hat{r}/l = 1$, $\hat{\theta} = |\theta_h|/2$.

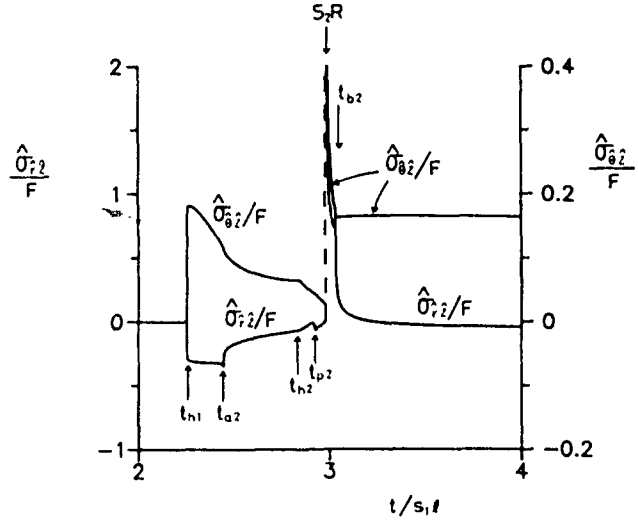

Fig. 8. Radiated stress history for anti-symmetric loading ($F_1 = -F_2 \equiv F$) at $\hat{r}/l = 1$, $\hat{\theta} = \theta_h/2$.

9. CONCLUSION

In this paper we have examined the elastodynamic responses of a crack along the interface of two anisotropic half planes. The responses are caused by a pair of anti-plane point loadings acting on the crack faces but located away from the crack tip. The solution was obtained by integral transforms together with the direct application of the Wiener–Hopf technique and the Cagniard–de Hoop method, which were previously believed not to be appropriate. The stress intensity factors and the radiated stress fields were found. Numerical results are presented for both the cases of anti-symmetric and symmetric point loadings.

The results show that the transient mode-III stress intensity factors, $\hat{K}_{III}$, are almost constants with time, but experience discontinuities at a time $t = s_2 l$, which is the arrival time of the cylindrical wave emitted from the point loading of the slower medium to the crack tip. Moreover, $\hat{K}_{III}$ jumps to the appropriate static value at $t = s_2 l$ in the case of anti-symmetric loading. On the other hand, it approaches the appropriate static value quite slowly in the case of symmetric loading. The results also show that the transient radiated stress component $\hat{\sigma}_{\hat{\theta}\hat{z}}$ has fewer discontinuities and fewer singularities than other stress components. Meanwhile, the order of magnitude of $\hat{\sigma}_{\hat{\theta}\hat{z}}$ is less than that of $\hat{\sigma}_{\hat{r}\hat{z}}$ by one.

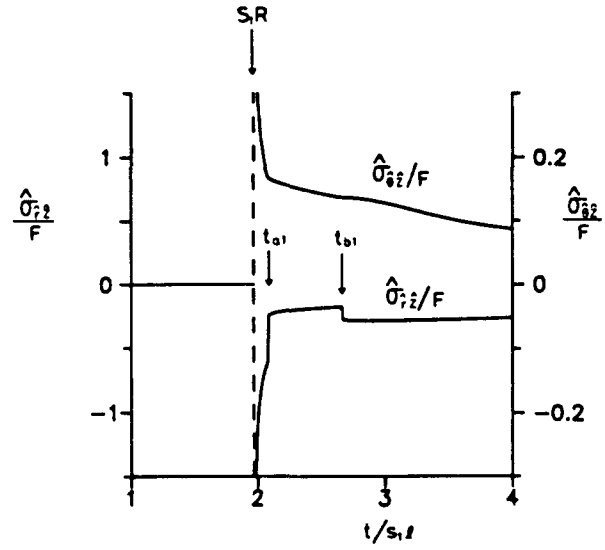

Fig. 9. Radiated stress history for symmetric loading ($F_1 = F_2 \equiv F$) at $\hat{r}/l = 1$, $\hat{\theta} = |\theta_h|/2$.

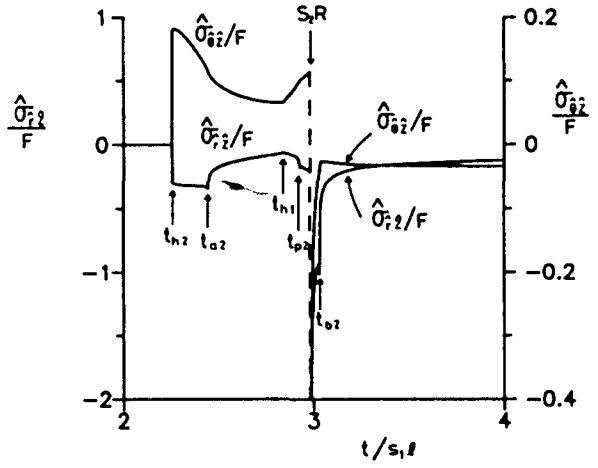

Fig. 10. Radiated stress history for symmetric loading ($F_1 = F_2 \equiv F$) at $\hat{r}/l = 1$, $\hat{\theta} = \theta_h/2$.

Acknowledgements—The authors would like to thank John Dempsey for bringing W. S. Ament's report to their attention. This work was sponsored by the National Science Council of the Republic of China under Grant NSC79-0401-E002-06.

REFERENCES

Achenbach, J. D. (1973). *Wave Propagation in Elastic Solids*. North-Holland, New York.

Achenbach, J. D. and Kuo, M. K. (1986). Effect of transverse isotropy on strong ground motion due to strike slip faulting. In *Earthquake Source Mechanics* (Edited by S. Das *et al.*), pp. 111–120. American Geophysical Union, Washington.

Ament, W. S. (1954). Application of a Wiener-Hopf technique to certain diffraction problems. NRL report 4334.

Brock, L. M. (1982). Shear and normal impact loadings on one face of a narrow slit. *Int. J. Solids Structures* **18**, 467–477.

Brock, L. M. and Achenbach, J. D. (1973). Extension of an interface flaw under the influence of transient waves. *Int. J. Solids Structures* **9**, 53–68.

Crampin, S. (1981). A review of wave motion in anisotropic and cracked elastic media. *Wave Motion* **3**, 343–392.

England, A. H. (1965). A crack between dissimilar media. *J. Appl. Mech.* **32**, 400–402.

Freund, L. B. (1974). The stress intensity factor due to normal impact loading on the faces of a crack. *Int. J. Engng Sci.* **12**, 179–190.

Freund, L. B. (1976). The analysis of elastodynamic crack tip stress fields. In *Mechanics Today* (Edited by S. Nemat-Nasser), Vol. 3, pp. 55–91. Pergamon Press, New York.

Georgiadis, H. G. (1986). Complex-variable and integral transform methods for elastodynamic solutions of cracked orthotropic strips. *Engng Fract. Mech.* **24**, 727–735.

Helbig, K. (1983). Elliptical anisotropy—its significance and meaning. *Geophysics* **48**, 825–832.
Ma, C. C. (1989) Analysis of dissimilar anisotropic wedges subjected to anti-plane shear deformation. *Int. J. Solids Structures* **25**(11), 1295–1309.
Markenscoff, X. and Ni, L. (1984). The transient motion of a screw dislocation in an anisotropic medium. *J. Elasticity* **14**, 93–95.
Noble, B. (1958). *Methods Based on the Wiener–Hopf Technique*. Pergamon Press, New York.
Sih, G. C. and Chen, E. P. (1981). *Cracks in Composite Materials*. Martinus Nijhoff, New York.
Wu, K. C. and Chiu, Y. T. (1990). Anti-plane shear interface cracks in anisotropic bimaterials, to appear in *J. Appl. Mech.*